Synthesis and high-temperature properties of *medium-entropy* (Ti,Ta,Zr,Nb)C using the spark plasma consolidation of carbide powders

D. Demirskyi (a,b,c)†, T.S. Suzuki (b), K. Yoshimi (c), and O. Vasylkiv (b)†.

(a) WPI-Advanced Institute for Materials Research (WPI-AIMR), Tohoku University, 2-1-1 Katahira, Aoba-ku, Sendai, 980-8577 Japan
(b) National Institute for Materials Science, 1-2-1 Sengen, Tsukuba, Ibaraki 305-0047, Japan
(c) Department of Materials Science and Engineering, Tohoku University, 6-6-02 Aramaki Aza Aoba, Sendai, 980-8579, Japan

Abstract

In this study, we explore a simple and effective method for producing a quaternary solid-solution of carbides, a medium-entropy $(Ti_{1/4}Ta_{1/4}Zr_{1/4}Nb_{1/4})C$. Using commercially-available carbide powders with an equimolar ratio and performing spark plasma consolidation at 1927 °C and 1977 °C, we demonstrated that the phase formation and high-temperature flexural strength can be controlled using the processing conditions. The flexural strength and fracture toughness at room temperature were reached an average of 560 MPa and 3.2 MPa $m^{1/2}$, respectively. The high-temperature performance of these ceramics was analyzed and compared with the available data for the group IV and V transition metal carbide monoliths.

Keywords: transition metal carbides; high-entropy ceramics; medium-entropy ceramics; flexural strength; high-temperature materials.

1 Introduction

Recent interest in devices capable of withstanding high temperatures concerns various industries from aerospace with advanced thermal protection materials to energy-related where an increase in energy efficiency is derived from an increase in the working temperatures. Energy efficiency is now being prioritized as new materials are being developed for green energy sources such as solar energy [1–3]. For these purposes, a class of ultra-high temperature ceramics (UHTC) is being used as the main backbone for future high-temperature material development. This is not surprising since monolithic additive-free carbides and diborides of

† Authors to whom correspondence should be addressed, Dmytro Demirskyi, demirskyi.dmytro.e2@tohoku.ac.jp /phone +81(0)70-2010-6281, Oleg Vasylkiv oleg.vasylkiv@nims.go.jp

the transition metals of the IV and V groups possess a unique combination of high melting points, high elastic moduli, and high-temperature strength [4–7].

To further increase the potential application of these compounds, further development is required as room and high-temperature performance of these monoliths is being constantly improved by the composite approach [8,9] or creating solid solutions [10]. The latter approach was spurred on by the development of multi-metal solid-solution compounds, analogous to the recent advances in metallurgy as these compounds were defined as high-entropy ceramics [11–13], while the equimolar solid-solution with four principle metal elements can be defined as medium-entropy ceramics.

Various synthesis methods for these carbides, borides, and silicides have been developed in the last two years [11–14]. However, because of the slow atomic mobility of transition metal carbides of the IV and V groups, their consolidation or combined consolidation/synthesis [11,13–16] requires a temperature range typical for the classical UHTCs (i.e., >1800 °C). Without careful control of the consolidation conditions, such high-temperatures cause grain growth and hence further embrittlement of these ceramics.

Despite reports of the high-hardness and high Young's modulus of high-entropy carbides, studies related to strength or toughness at room or high-temperature are somewhat sparse [14,16–19].

A recent report of the ternary high-entropy carbide prototype $(Ta_{1/3}Zr_{1/3}Nb_{1/3})C$ [14] showed an interesting high-temperature flexural behavior, suggesting that solid-solution strengthening might lead to further improvement of the high-temperature properties. In this regard, further studies, which investigate the addition of a 4^{th} or 5^{th} metal atom to the (Ta,Zr,Nb)C system may clarify the potential in the development of carbides in particular, and the UHTC in general.

In the present study to obtain a quaternary medium-entropy carbide, the TiC, TaC, ZrC, and NbC were combined at the mixing stage. The formation of a solid-solution between carbides was observed during the spark plasma consolidation at 1927 °C and 1977 °C. The present investigation will examine the possibility of using these ceramics as a structural material at elevated temperatures (i.e, 1600–1800 °C). In particular, the effect of the processing conditions on the lattice parameters and high-temperature flexural strength were the main focus of this study.

2 Materials and Methods

Commercially available TiC, TaC, ZrC, and NbC (Wako Pure Chemicals, Osaka, Japan) powders were used as the starting materials. The raw powders were mixed in equimolar ratios TiC:TaC:ZrC:NbC 1:1:1:1. Powder mixtures were prepared by wet-chemical mixing in alcohol with low-temperature drying (at ~100 °C) to remove moisture. The resultant powder was screened using a 60-mesh screen. For simplicity, a quaternary equimolar mixture was denoted as TTZN. Based on the previous results for (Ta,Zr,Nb)C [14], a dwell time of 10 and 40 min at 1977 °C and 1927 °C was used: TTZN–10 and TTZN–40, respectively. These conditions were used in order to obtain ceramics with similar grain sizes.

The spark plasma sintering (SPS) experiments were conducted using 'Dr. Sinter' 1050 (Sumitomo, Japan) unit using a 30-mm die. The schedule for the TTZN carbide specimens prepared in this study had four major steps: (1) heating to 700 °C in four minutes following a five-minute dwell, (2) heating to 1500 °C in 10 minutes with a five-minute dwell; (3) five-minute ramp to 1927 °C or 1977 °C, with a dwell of 40 or 10 minutes. The last step included cooling down to 600 °C in 15 minutes. Steps (1) and (2) were performed in a vacuum; during the dwell at 1400 °C, the SPS chamber was backfilled with argon. At the end of the dwell at stage (2), the pressure was increased from 8 to 12 kN, while reaching 1927 °C the pressure was increased from 12 to 32 kN. The pressure of 32 kN was maintained during the consolidation and cooling stages. Argon gas at the flow rate of 2 L/min was used.

An X-ray diffraction (XRD) analysis (D8 Advance, Bruker, Karlsruhe, Germany) was performed on the polished surfaces of the bars before the flexural tests using the Cu-Kα radiation. The intensity data were collected over the 2θ range of 20°– 130°, in steps of 0.02–0.05°, using a sampling time of 10 s for each step. In some instances, a sampling time of 40 s was used in the attempt to refine peaks with 2 thetas higher than 100°. The software used for the refinement was TOPAS (TOPAS Ver. 4.0, Bruker AXS, Germany). Instrumental broadening was determined using a NIST 660b LaB_6 standard is run under the same conditions for each carbide sample [20]. The computation of the lattice parameters for the NaCl-type carbides was performed using TOPAS or using refinement code developed by Lutterotti et al. [21]. Lattice parameters of the carbides were determined with an accuracy of 0.0001 Å.

The structural characteristics of the TTZN ceramics and were studied using scanning electron microscopy (SEM, JCM-6000, JEOL) with secondary (SE) and backscattered electrons (BSE mode).

The three-point flexural strength was determined using rectangular blocks (2×2×25 mm) using strength testing equipment were previously described in detail [22,23]. A span of 16 mm was used. Measurements were performed with a loading speed of 0.5 mm/min. Four to six samples

were tested at room temperature originated from ceramic tiles that were free of macroscopic cracks. In some instances, specimens were tested using the four-point method (a 20–10 mm configuration). The standard deviation was taken as the measurement accuracy. Tests at elevated temperatures were performed in argon. The heating procedure for the high-temperature flexure tests at 1600 °C and 1800 °C are described in detail elsewhere [23].

We evaluated the elastic modulus (Ef) for the tests at room temperature from the linear portion of the load-displacement curve using the procedure described in ASTM E111–04.

The fracture toughness of the ceramics was evaluated using specimen bending testing which contained a single edge through-thickness notch following ASTM C1421–10. Details of the testing configuration and the notch profile are presented in ref. [8]. Two tests with loading rates of 0.05 and 0.5 mm/min were performed.

Hardness was determined by an MMT-7 Vickers hardness tester (Matsuzawa MMT-7; Matsuzawa SEIKI Co., Ltd., Tokyo, Japan), using load 9.8 N with a dwell time of 15 s following the standard procedure (ASTM C 1327–15).

3 Results and Discussion

3.1 Structure analysis of medium-entropy carbide ceramics

Figure 1 shows a summary of the XRD analysis performed within the present study. One can see that in the case of the TTZN–40 (**Fig. 1 (b)**), a single-phase ceramic was formed. In the case of the shorter dwell time (TTZN–10), the presence of two phases was suggested based on the refinement results (**Table 1**). In this case, two phases were identified as quaternary carbides with lattice parameters of a = 4.4816 Å and a = 4.4687 Å. The lattice parameter of the quaternary TTZN–40 phase in **Fig. 1 (b)** was estimated to be 4.4687 Å. In this case structural refinement presented in **Table 1** for the phase designated as TTZN–10_2 is valid for both the TTZN–10 and TTZN–40 specimens.

The difference in phases between the TTZN–10 and TTZN–40 ceramics is more obvious during the analysis of the (442) peak (**Fig. 1 (c)**). For clarity, the Kα2 peaks were not removed from the data presented in **Fig. 1**. For the case of the TTZN–40, both the Kα1 and Kα2 peaks are visible even using a 0.05° step size, while for the TTZN–10, a 0.02° step size and 40 s sampling time does not allow separating these peaks. Thus it is postulated [20] that at least two carbide phases are present for the TTZN–10 ceramic. Furthermore, the phase (TTZN–10_1 in **Table 1**) with the lattice parameter a = 4.4816 Å suffers from the severe contribution of strain and misorientation [24].

The difference between the phases based on the refinement results, and taking into account the results of the EDX analysis (see below) can be understood based on the occupancy of the Ti atom in the quaternary solid-solution (**Table 1, Fig. 2**). The theoretical density of the TTZN specimens was estimated as 8.353 and 8.408 g/cm^3. The bulk densities of the SPSed TTZN ceramics are 8.31 g/cm^3 (10 min dwell at 1977 °C) and 8.35 g/cm^3 (40 min dwell at 1927 °C). Another detail was derived during the XRD analysis – a quasi-linear correlation between the reported lattice parameters and the theoretical density for the medium-entropy/high-entropy carbide ceramics (see **Fig. 1 (d)**) [14–16,19,25–27]. One can see a clear difference between the medium-entropy (i.e. <5 principle elements), high-entropy [14,15,25–27] and binary carbides [28,29] based on the two lines obtained using the regression analysis in Origin 7.5 (OriginLab Corp.). This difference serves as an indication of the order/disorder in the complex solid solution, but further confirmation based on compounds with a similar NaCl-type structure, e.g., nitrides, is required.

The SEM micrographs for the ceramic bulks after the flexural tests at room temperature (**Figs. 3,4**) illustrate the difference between the TTZN–10 and TTZN–40 ceramics that were consolidated using different conditions. The TTZN–10 ceramic consists of at least two carbide phases, while the TTZN–40 was found to be a single-phase ceramic. In the case of the TTZN–10 ceramic (**Figure 3**), it was possible to identify the Ti-rich (Ti – 30 mol.%; Ta, Zr, Nb – 23 mol.%) and equimolar sold-solution phases (Ta,Ti, Zr, Nb – 25 mol.%) using EDX. The titanium-rich quaternary carbide phase occupied up to 32 vol.% which is in rough agreement with 42.5 vol.% based on the XRD refinement.

In terms of the fractographic analysis (using ImageJ, OrientationJ), after the flexural tests at room temperature, a mixed fracture mode was observed for TTZN–10 and TTZN–40. For the TTZN–10 ceramic, one can see the larger contribution of the transgranular fracture mode compared to the TTZN–40 ceramic. Nevertheless, in both cases, one can observe the presence of microcracks even after the tests at 1800 °C [14]. The mean grain size for the TTZN–10 and TTZN–40 ceramics was 19±4 μm and 15±4 μm, respectively. In some instances fine grains were observed for both ceramics with a grain size between 8 and 12 μm (up to 10 vol.%). Grains exceeding 25 μm were extremely rare. Pores had a spherical shape and size between 1 and 2 μm. The total porosity based on the fractographic analysis was less than 1 vol.%.

3.2 Mechanical properties at room temperature

Hardness of the bulk TTZN–10 and TTZN–40 ceramics was within 27.6±2.3 GPa, comparable to that reported in refs. [14,18], but somehow higher than in [16]. In terms of the development

of quaternary or quintenary high-entropy carbides as a structural material for the high-temperature applications, further optimization of the processing may be required. For the TTZN ceramics, within the eight specimens attempted, only five were free of macroscopic cracks [14,30]. Thus, it is thought that micro- and macrocracking is the reason for the absence of the flexural strength data for these compounds. Because, even within the present study, only specimens free of macroscopic cracks were used for the flexural tests (~40% of the specimens had macroscopic cracks after SPS). Further optimization of the consolidation process is a mandatory step to decrease the grain size (to at least 10 μm) in order to control the mechanical performance and cracking issue [30,31].

For the crack-free specimens of the TTZN–40 ceramic, the flexural strength and fracture toughness at room temperature were 544±35 MPa and 3.2±0.2 MPa $m^{1/2}$, respectively. For the TTZN–10 ceramic, a slightly higher average strength was evaluated as 560±49 MPa, while the toughness was 3.3±0.2 MPa $m^{1/2}$. In absolute values, the strength of the ($Ti_{1/4}Ta_{1/4}Zr_{1/4}Nb_{1/4}$) carbide ceramics are on the same level as reported for the TaC or TaB_2 ceramics [32–38]. However, because the formation of the medium-entropy or high-entropy ceramics allows controlling the bulk density, the values of the specific strength were higher than those for the TaC ceramics. Furthermore, one can see from **Fig. 5** [14,16,31–48] that TTZN–10 has a slightly higher absolute or specific strength compared to TTZN–40. This can be explained in terms of the presence of the second phase that might act as strengthening elements, and, of course, due to the formation of the solid solution and local stresses associated with the lattice distortion.

3.3 Analysis of high-temperature properties

As a rule for the monolithic single phase ceramic, the presence of segregated impurities or secondary phases may greatly influence the flexural strength at room temperature or at elevated temperature. Thus in the following analysis, the data for the additive-free ceramics are being used. Nevertheless, it should be noted that, if possible, the grain size reported by the authors of the original study was mentioned. These actions were made to minimize the possibility for incorrect data interpretation during analysis that is provided below.

It should be noted that the data for the UHTC-based ceramic composites and monolithic UHTC may be differently interpreted [1,2,4]. The addition of a even minor amount of secondary reinforcement phase (SiC, WC, WB, $MoSi_2$, etc) to the UHTC matrix will have its own toughening or strengthening advantages [1–4]. Hence, when the monolithic carbide/diboride is being improved by creation of a solid-solution and by adding a reinforcement phase, the

strengthening effect is more difficult to explain [4]. In the case of the studies of the monolithic (circa free of SiC, B_4C or $MoSi_2$, etc., additives) carbide or boride ceramics [4,31], it may be suggested that the strength improvement associated with the solid-solution formation for these monolithic ceramics can be (i) lost upon reheating to higher temperatures, (ii) maintained up to a higher temperature region, or (iii) can be suppressed by the contribution of local plastic deformation [14, 31] before the significant decrease in strength would occur due to macroscopic plastic deformation.

In this regard, one of the main goals of the present study was to analyze the high-temperature behavior of the medium-entropy ($Ti_{1/4}Ta_{1/4}Zr_{1/4}Nb_{1/4}$) carbide compared with data for other monolithic carbides (**Figs. 6–12**) [14, 31–62]. Our previous attempt for the ternary ($Ta_{1/3}Zr_{1/3}Nb_{1/3}$) carbide [14] suggested that the behavior of the ternary ceramic is comparable with data for the pure NbC [48,49] or NbC–ZrC [50] solid solution as their behavior is quite similar at elevated temperatures. The only difference was the onset of the significant contribution of the macroscopic plastic deformation, which was slightly higher for the NbC–ZrC case [50].

The results of the present study may provide an additional explanation for these observations. First, for the TTZN–10 or TTZN–40 ceramics, a decrease in strength was noticeable at 1000 °C, which can be explained as an effect of the reheating. The degree of strength degradation or strength vs the temperature dependence was different for the two medium-entropy carbide ceramics. This becomes clear after examination of **Figure 6 (b)**, in which the data for the low-temperature region of the TTZN–10 ceramic are approximated using the dashed line. One can see that in terms of the flexural strength at 1600 °C, the ($Ta_{1/3}Zr_{1/3}Nb_{1/3}$) carbide [14] and TTZN–10 have similar strength. Nevertheless, the (Ta,Zr,Nb) carbide shows a gradual increase in strength. Because this trend is similar to that for the NbC–ZrC data [50] (see **Fig. 7** [14,36,40,41,48–51]), it was concluded in [14] that this may be due to the governing role of the solid-solution strengthening with respect to the flexural strength behavior of the single-phase medium-entropy (Ta,Zr,Nb) carbide.

Data for the temperature dependence of the individual monolithic carbides of the IV and V groups with the NaCl-type lattice are summarized in **Figures 8–12** [36,40–44,47–49,51–62]. Although HfC was not used in the present study, we attempted to analyze the data for the monolithic hafnium carbide since we consider the addition of HfC to study the (Ta,Zr,Nb,Hf)C, (Ti,Zr,Nb,Hf)C and (Ti,Ta,Zr,Nb,Hf)C carbide ceramics.

The high-temperature flexural behavior of titanium carbide (**Figure 8**) [40–43,52] can be summarized as follows: a slight variation in strength before 1400–1500 °C (brittle to ductile

transition temperature, BDTT), followed by a rapid strength decrease due to activation of the macroscopic plastic deformation [31,63]. TaC also follows a similar trend (see **Figure 11**[48,49,51,52,58]), but a study [59] reported a deep minimum at 1400 °C, followed by an increase in strength. Data for the BDTT of tantalum carbide showed quite a wide range from 1550 °C to 2300 °C [49,61,64,65]. Similar to the flexural strength, the BDTT is sensitive to a carbon deficiency [65], method of fracture, consolidation or annealing conditions, and strain rates [64].

The data for ZrC [44,47,51,53,54] and NbC [48,49,51,52,58] are slightly different, and they are fully discussed in the study of ref. [31]. For these ceramics, the transition between brittle and ductile fracture is associated with a bell-shaped strength dependence (i.e., with a clear maximum). The peak strength for these ceramics is usually observed in the vicinity of the BDTT, but the position of the peak is quite sensitive to (a) grain size and (b) consolidation conditions, i.e., a higher consolidation temperature allows shifting the peak strength to higher temperatures. Flexural strength data for HfC are scarce [55–57]. Within the available sources, two studies indicate a dependence typical for TiC, but one study [57] reported a gradual increase in strength up to 2200 °C. As noted above, data of the flexural strength of binary carbides are limited by [50], in which the NbC–ZrC solid-solution follows a trend similar to the individual NbC or ZrC. Based on these results, one can underline the importance of studies about binary carbides and carbides featuring HfC, as an increase in strength after 2000 °C for the monolithic HfC reported in refs. [55] and [57] looks quite interesting from theoretical and practical viewpoints.

The shaded strength window highlighted in **Fig. 7** [14,36,40,41,48–51] serves as an indication of an abnormal strength behavior and perhaps is best suited for the practical applications of these compounds. Typical loading curves at 1600 °C and 1800 °C suggest that a fully elastic behavior is observed for the TTZN ceramics at 1600 °C, while a deviation from elastic behavior serves as an indication of the ongoing plastic deformation at 1800 °C [21,35,63]. The yield stress instead of fracture stress was used for the analysis in **Fig. 6** of specimens tested at 1800 °C.

As noted above, both data sets in this study show a gradual decrease in strength, thus one can interpret this situation in terms of the magnitude of the local stresses stored and released upon reheating to high temperatures. Because of the relatively high flexural strength at room temperature observed for the TTZN carbides within this study (>500 MPa, comparable to bulk TaC [32,34,36]), it is suggested that the thermal history of the specimens during consolidation allowed activation accumulation of a higher lattice strain, which was relaxed at the higher

temperatures. Microcracking was reported to be visible even at 2000 °C for the (Ta,Zr,Nb) carbide [14]. Because the appearance of microcracks was noticed at temperatures above 1600 °C for (Ti,Ta,Zr,Nb) carbides within the present study, it may be suggested that only high-temperature annealing above >2000 °C may help one to understand the exact mechanism of the stress relaxation. Furthermore, for the binary carbide systems, a miscibility gap may differ from 1880 °C to 2050 °C for the TiC–HfC system [66], while the miscibility gap for the ternary $(TiC)_{0.27}(HfC)_{0.41}(WC)_{0.32}$ system was studied at 1540 °C [66,67]. As noted in ref. [67], the binary, ternary and multi-carbides of the metals of the IV and V groups (excluding VC) addition of NbC, in particular to the ternary system may expand the single-phase limit after a 2000 °C/12h annealing.

Another important observation that was made during the high-temperature flexural strength is that Young's modulus degradation for the medium-entropy TTZN carbides was not as severe as for the monolithic carbides. Following the analysis of ref. [68], **Figure 13** shows the evolution of the specific stiffness (based on Ef values) and absolute values of Young's modulus at room temperature and at 1600 °C [4,5,68]. Data for the (Ti,Ta,Zr,Nb)C carbides favorably agree with the modulus of the TaC data, but as noted previously due to a sufficient decrease in the theoretical density, the TTZN ceramics have a higher specific stiffness. HEC stands for data on elastic moduli at room-temperature data from ref. [19] (data for carbides with valence electron concentration between 8.6 and 9 were used). Furthermore, a slight deviation from the equimolar ratio observed for the TTZN–10 ceramic phases (**Fig. 1**, **Table 1**) may also contribute to the higher modulus values as was noted that for some binary carbide systems, the maximum in modulus or creep-resistance was observed for the 40/60 values rather than the 50/50 value, as the former concentration is believed to be responsible for the maximum in the distortion of the crystal lattice [4,69].

This underlines the fact that for medium-entropy or high-entropy carbide ceramics, the effect of the processing conditions (at least for an *in situ* approach [13,14]) can be tailored to govern the solid-solution strengthening and to manufacture carbide ceramics with a high strength and high stiffness up to 1600 °C. The contribution of various factors can be further optimized but required an in-depth knowledge of the carbides behavior for ternary, quaternary, and quintenary equimolar carbide systems.

To understand the effect of the solid-solution, it is suggested that high-entropy ceramics with different grain sizes should be manufactured similar to study [16]. This underlines the importance of further consolidation kinetic studies of these ceramics. These studies and high-

temperature characterization of the equimolar (Ta,Zr,Nb,Hf)C, (Ti,Zr,Nb,Hf)C and (Ti,Ta,Zr,Nb,Hf)C carbide ceramics are considered as a crucial step in the ongoing research.

4 Summary and conclusions

Bulk solid-solution or medium-entropy carbide ceramics have been obtained by two different thermal histories using the spark plasma sintering method. Phase analysis via lattice parameter measurements by X-ray diffraction showed the processing conditions such as dwell time and consolidation temperature, allow one to produce single-phase or multi-phase carbide ceramics with the lattice parameters of the phases of a = 4.4816 Å and a = 4.4687 Å.

The mechanical performance at room temperature for the (Ti,Ta,Zr,Nb) carbides is comparable to the best data for the TiC or TaC monolithic ceramics, reaching 600 MPa. This may be explained in terms of a solid-solution strengthening mechanism. In terms of the specific flexural strength or specific stiffness, medium-entropy carbide bulks are superior to the majority of the monolithic carbides, except the TiC. Titanium carbide is known to have a brittle to ductile transition temperature around 1200–1300 °C, which does not allow using it as per se high-temperature ceramics. Importantly, at elevated temperatures, medium-entropy (Ti,Ta,Zr,Nb) carbides possess the strength of 300 or 500 MPa at 1600 °C where they fracture in an elastic manner. The strength at high temperatures depends on the consolidation conditions. Based on the results of this study, consolidation using a higher temperature but shorter dwell time is recommended.

Acknowledgements

Authors express their sincere appreciation to Dr. Toshiyuki Nishimura (NIMS) for providing access to the evaluation of high-temperature strength, this study would not be as complete otherwise.

D.D. was supported by World Premier International Research Center Initiative (WPI), MEXT, Japan.

References

[1] W.G. Fahrenholtz, G.E. Hilmas, I.G. Talmy, J.A. Zaykoski, Refractory Diborides of Zirconium and Hafnium, J. Am. Ceram. Soc. **90** (2007) 1347–1364. https://doi.org/10.1111/j.1551-2916.2007.01583.x

[2] W.G. Fahrenholtz, E.J. Wuchina, W.E. Lee, Y. Zhou Y (Eds.), Ultra-high temperature ceramics, Wiley, Hoboken, N.J., 2014.

[3] L.Silvestroni, D. Sciti, L. Zoli, A. Balboa, et al., An overview of ultra-refractory ceramics for thermodynamic solar energy generation at high temperature, Renewable Energy **133** (2019) 1257–1267. https://doi.org/10.1016/j.renene.2018.08.036.

[4] R.A. Andrievski, I.I. Spivak, Strength of Refractory Compounds, Metallurgiya, Chelyabinsk, 1989, [in Russian].

[5] T.Ya. Kosolapova, Properties, synthesis and application of refractory compounds, Reference Book, Metallurgiya, Moscow, 1986, [in Russian],

[6] L.E. Toth. Transition Metal Carbides and Nitrides, Academic Press, New York, 1971.

[7] J. Castaing, P. Costa, Properties and uses of diborides. in: V.I. Matkovitch, G.V. Samsonov, P. Hagenmuller, T. Lundstrom (Eds.), Boron and Refractory Borides, Springer-Verlag, Berlin, Heidelberg, N.Y., 1977, pp. 390–412. https://doi.org/10.1007/978-3-642-66620-9_22.

[8] D. Demirskyi, O. Vaslykiv, Spark plasma sintering and high-temperature strength of B6O–TaB2 ceramics, J. Eur. Ceram. Soc. **37**[8] (2017) 3009–3014. https://doi.org/10.1016/j.jeurceramsoc.2017.02.052.

[9] T.H. Squire, J. Marschall, Material property requirements for analysis and design of UHTC components in hypersonic applications, J. Eur. Ceram. Soc. **30**[11] (2010) 2239–2251. https://doi.org/10.1016/j.jeurceramsoc.2010.01.026.

[10] C. Mroz, Processing TiZrC and TiZrB2, Am Ceram. Soc. Bull. 73 (1994) 78–81.

[11] E. Castle, T. Csanadi, S. Grasso, J. Dusza, M. Reece, Processing and Properties of High-Entropy Ultra-High Temperature Carbides, Sci. Rep. **8** (2018) 8609. https://doi.org/10.1038/s41598-018-26827-1.

[12] P. Sarker, T. Harrington, C. Toher, et al., High-entropy high-hardness metal carbides discovered by entropy descriptors, Nat. Commun. 9 (2018) 4980. https://doi.org/10.1038/s41467-018-07160-7.

[13] C. Oses, C. Toher, S. Curtarolo, High-entropy ceramics, Nat. Rev. Mater. (2020). https://doi.org/10.1038/s41578-019-0170-8.

[14] D. Demirskyi, H. Borodianska, T.S. Suzuki, Y. Sakka, K. Yoshimi, O. Vasylkiv, High-temperature flexural strength performance of ternary high-entropy carbide consolidated via spark plasma sintering of TaC, ZrC and NbC, Scr. Mater. 164 (2019) 12–16. https://doi.org/10.1016/j.scriptamat.2019.01.024.

[15] X.-F.Wei, J.-X. Liu, F. Li, Y. Qin, Y.-C. Liang, G.-J. Zhang, High entropy carbide ceramics from different starting materials, J. Eur. Ceram. Soc. **39**[10] (2019) 2989–2994. https://doi.org/10.1016/j.jeurceramsoc.2019.04.006.

[16] F. Wang, X. Zhang, X. Yan, Y. Lu, M. Nastasi, Y. Chen, B. Cui, The effect of submicron grain size on thermal stability and mechanical properties of high- entropy carbide ceramics, J. Am. Ceram. Soc. 103 (2020) 4463–4472. https://doi.org/10.1111/jace.17103.

[17] T. Csanadi, E. Castle, M.J. Reece, et al., Strength enhancement and slip behaviour of high-entropy carbide grains during micro-compression, Sci. Rep. 9 (2019) 10200. https://doi.org/10.1038/s41598-019-46614-w.

[18] K. Wang, L. Chen. C. Xu, W. Zhang, Z. Liu, Y. Wang, J. Ouyang, X. Zhang, Y. Fu, Y. Zhou, Microstructure and mechanical properties of (TiZrNbTaMo)C high-entropy ceramic, J. Mater. Sci. Technol. **39**[15] (2020) 99–105. https://doi.org/10.1016/j.jmst.2019.07.056.

[19] T.J. Harrington, J. Gild, P. Sarker, C. Toher, C.M.O.F. Dippo, C. McElfresh, K. Kaufmann, E. Marin, L. Borowski, P.E. Hopkins, J. Luo, S. Curtarolo, D.W. Brenner, K.S. Vecchio, Phase stability and mechanical properties of novel high entropy transition metal carbides, Acta Mater. **166** (2019) 271–280. https://doi.org/10.1016/j.actamat.2018.12.054.

[20] B.D. Cullity Elements of X-Ray Diffraction, 2nd Ed., Addison-Wesley Publishing Inc., Reading, MA, 1978.

[21] L. Lutterotti, H. Pilliere, C. Fontugne, P. Boullay, D. Chateigner, Full-profile search-match by the Rietveld method. J. Appl. Crystallogr. **52** (2019) 587–598. https://doi.org/10.1107/S160057671900342X.

[22] D. Demirskyi, O. Vasylkiv, Analysis of the high-temperature flexural strength behavior of B4C–TaB2 eutectic composites produced by in situ spark plasma sintering, Mater. Sci. Eng. A 697 (2017) 71–78. https://doi.org/10.1016/j.msea.2017.04.093.

[23] D. Demirskyi, Y. Sakka, O. Vasylkiv, High-Strength B4C–TaB2 Eutectic Composites Obtained via In Situ by Spark Plasma Sintering, J. Am. Ceram. Soc. 99 [7] (2016) 2436–2441. https://doi.org/10.1111/jace.14235.

[24] I.Borgh, P.Hedström, A.Blomqvist, J.Ågren, J. Odqvist, Synthesis and phase separation of (Ti,Zr)C, Acta Mater. **66** (2014) 209–218. https://doi.org/10.1016/j.actamat.2013.11.074.

[25] D. Liu, A. Zhang, J. Ji, J. Meng, B. Su, Phase evolution and properties of (VNbTaMoW)C high entropy carbide prepared by reaction synthesis, J. Eur. Ceram. Soc. 40 (2020) 2746–2751. https://doi.org/10.1016/j.jeurceramsoc.2020.03.020.

[26] B. Ye, T. Wen, M. C. Nguyen, L. Hao, C.-Z. Wang, Y. Chu, First-principles study, fabrication and characterization of (Zr0.25Nb0.25Ti0.25V0.25)C high-entropy ceramics, Acta Mater. **170** (2019) 15–23. https://doi.org/10.1016/j.actamat.2019.03.021.

[27] S. Jiang, L. Shao, T.-W. Fan, J.-M. Duan, X.-T. Chen, B.-Y. Tang, Elastic and thermodynamic properties of high entropy carbide (HfTaZrTi)C and (HfTaZrNb)C from ab initio investigation, Ceram. Int. **46** (2020) 15104–15112. https://doi.org/10.1016/j.ceramint.2020.03.045.

[28] The International Centre for Diffraction Data (ICDD), PDF-2, Release 2004.

[29] The International Centre for Diffraction Data (ICDD), PDF-4, Release 2010.

[30] H.R. Baumgartner, R.A. Steiger, Sintering and properties of titanium diboride made from powder synthesized in a plasma-arc heater, J. Am. Ceram. Soc. **67** (1984) 207–212. https://doi.org/10.1111/j.1151-2916.1984.tb19744.x.

[31] P.V. Zubarev, High-temperature strength of the interstitial phases, Metallurgiya, Moscow, 1985, [in Russian].

[32] L. Silvestroni, L.Pienti, S. Guicciardi, D. Sciti, Strength and toughness: the challenging case of TaC-based composites, Composites: Part B **72** (2015) 10–20. https://doi.org/10.1016/j.compositesb.2014.11.043.

[33] J- X. Liu, Y.- M. Kan, G.- J. Zhang, Pressureless Sintering of Tantalum Carbide Ceramics without Additives, J. Am. Ceram. Soc., **93**[2] (2010) 370–373. https://doi.org/10.1111/j.1551-2916.2009.03437.x.

[34] X. Zhang, G.E. Hilmas, W.G. Fahrenholtz, Densification and mechanical properties of TaC-based ceramics, Mater. Sci. Eng. A **501** (2009) 37–43. https://doi.org/10.1016/j.msea.2008.09.024.

[35] K. Hackett, S. Verhoef, R.A. Cutler, D.K. Shetty, Phase constitution and mechanical properties of carbides in the Ta-C system, J. Am. Ceram. Soc. **92**[10] (2009) 2404–2407. https://doi.org/10.1111/j.1551-2916.2009.03201.x.

[36] D. Demirskyi, T. Nishimura, Y. Sakka, O. Vasylkiv, High-strength TiB2–TaC ceramic composites prepared using reactive spark plasma consolidation, Ceram. Int. **42** (2016) 1298–1306. https://doi.org/10.1016/j.ceramint.2015.09.065.

[37] D. Demirskyi, O. Vasylkiv, Consolidation and grain growth of tantalum diboride during spark plasma sintering, Ceram. Int. **42** (2016) 16396–16400. https://doi.org/10.1016/j.ceramint.2016.07.059.

[38] R. Licheri, C. Musa, R. Orru, G. Cao, D. Sciti, L. Silvestroni, Bulk monolithic zirconium and tantalum diborides by reactive and non-reactive spark plasma sintering, J. Alloy Compd. **663** (2016) 351–359. https://doi.org/10.1016/j.jallcom.2015.12.096.

[39] E. Zapata-Solvas, D.D. Jayaseelan, H.T. Lin, P. Brown, W.E. Lee, Mechanical properties of ZrB2- and HfB2-based ultra-high temperature ceramics fabricated by spark plasma sintering, J. Eur. Ceram. Soc. **33** (2013) 1373–1386. https://doi.org/10.1016/j.jeurceramsoc.2012.12.009.

[40] A.P. Katz, H.A. Lipsitt, T. Mah, M.G. Mendiratta, Mechanical behaviour of polycrystalline TiC, J. Mater. Sci. **18** (1983) 1983–1992. https://doi.org/10.1007/BF00554991.

[41] D.B. Miracle, H.A. Lipsitt, Mechanical Properties of Fine- Grained Substoichiometric Titanium Carbide, J. Am. Ceram. Soc. **66**[8] (1983) 592–597. https://doi.org/10.1111/j.1151-2916.1983.tb10098.x.

[42] Strength data of reference 574 in [5].

[43] Strength data of reference 636 in [5].

[44] P.V. Zubarev, A.B. Kuraev, Stress relaxation in zirconium carbide. 2. Mechanisms of stress relaxation. The relationship of the processes of creep and relaxation, Strength Mater. **26** (1994) 132–136. https://doi.org/10.1007/BF02209330.

[45] D. Sciti, S. Guicciardia, M. Nygren, Spark plasma sintering and mechanical behaviour of ZrC-based composites, Scr. Mater. **59** (2008) 638–641. https://doi.org/10.1016/j.scriptamat.2008.05.026.

[46] Strength data of reference 489 in [5].

[47] J. Zhao, J. Zou, Z.-Y. Man, X.-G. Wang, J.-X. Xue, G.-J. Zhang, Dopant effects on high temperature mechanical properties of zirconium carbide ceramics, Adv. Appl. Ceram. **114**(6) (2015) 338–343. https://doi.org/10.1179/1743676115Y.0000000001.

[48] S.S. Ordan'yan, E.K. Stepanenko, I.V. Sokolov, Strength of NbC-NbB2 sintered composites, Izv. Vyssh. Uchebn. Zaved., Khim. Khim T. 27[10] (1984):1201–1203.

[49] A. Kelly, D.J. Rowcliffe, Deformation of polycrystalline transition metal carbides, J. Am. Ceram. Soc. **50** (1967) 253–256. https://doi.org/10.1111/j.1151-2916.1967.tb15098.x.

[50] A.G. Lanin, P.V. Zubarev, K.P. Vlasov, Mechanical and thermophysical properties of materials in HTGR fuel bundles, Atom. Energy **74** [1] (1993) 40–44.

[51] Strength data of reference 542 in [4].

[52] Strength data of reference 500 in [5].

[53] Strength data of reference 485 in [5].

[54] Strength data of reference 580 in [5].

[55] W.A. Sanders, H.B. Probst, High-temperature mechanical properties of polycrystalline hafnium carbide and hafnium carbide containing 13 vol.% hafnium diboride. Report NASA-TN-D-5008. NASA Lewis Research Centre, Cleveland, Ohio, 1963.

[56] W.A. Sanders, J.R. Creagh, C. Zalabak, J.J. Gangler, Preliminary investigation of the fabrication and properties of hafnium carbide, in: G.M. Ault, W.F. Barclay, H.P. Munger (Eds.), High-temperature material II, Interscience Publishers, N.Y., 1961, pp. 469–483. Available via https://archive.org/details/nasa_techdoc_19630011490.

[57] Strength data of reference 634 in [5].

[58] Strength data of reference 610 in [5].

[59] R. Lowrie, Research on physical and chemical principles affecting high temperature materials for rocket nozzles. Quarterly Progress Report, Contract DA 30-069-ORD-2787. Union Carbide Research Institute, Tarrytown, New York, (1964).

[60] Strength data of reference 584 in [5].

[61] H.A. Johansen, J.G. Cleary, The ductile-brittle transition in tantalum carbide. J. Electrochem. Soc. **113**[4] (1966) 378–381. https://doi.org/10.1149/1.2423967.

[62] G.E. Hollox, Microstructure and mechanical behaviour of carbides, Mater. Sci. Eng. **3**[3] (1968/69) 121–137. https://doi.org/10.1016/0025-5416(68)90001-3.

[63] D. Demirskyi, O. Vasylkiv, Mechanical properties of SiC–NbB2 eutectic composites by in situ spark plasma sintering, Ceram. Int. **42**[16] (2016) 19372–19385. https://doi.org/10.1016/j.ceramint.2016.09.110.

[64] M. Hoffman, W.S. Williams, A simple model for the deformation behaviour of tantalum carbide, J. Am. Ceram. Soc. **69**[8] (1986) 612–614. https://doi.org/10.1111/j.1151-2916.1986.tb04817.x.

[65] G.V. Samsonov, G.S. Upadhyaya, V.S. Neshpor, Physical Materials Science of Carbides, Naukova Dumka, Kiev, Ukraine, 1974, [In Russian].

[66] Z. Huang, L. Wu, Phase Equilibria Diagrams of High Temperature Non-oxide Ceramics, Springer, Singapore, 2018.

[67] R. Kieffer, F. Benesovsky, Hartstoffe, Springer, Wien, 1963, [in German].

[68] W.B. Hillig, Prospects for Ultrahigh-Temperature Ceramic Composites, in: R.E. Tressler, G.L. Gessing, C.G. Pantano, R.E. Newnham (Eds.), Tailoring Multiphase and Composite Ceramics, Plenum Press, 1986, pp. 697–712. https://doi.org/10.1007/978-1-4613-2233-7_55.

[69] Analysis of strength data of reference 455 in [4].

Tables

Table 1. Results of structure refinement of carbide phases for TTZN–10 ceramic.

Designation	TTZN–10_1	TTZN–10_2 [Y]
Lattice parameter, Å	4.4816	4.4687
Ti occupancy	0.2400	0.2755
Ta occupancy	0.2582	0.2410
Zr occupancy	0.2568	0.2417
Nb occupancy	0.2569	0.2416
C occupancy*	1	1
Rwp / GOF	4.7 / 2.2	

* fixed to 0.99 during structure refinement

[Y] main phase for the TTZN–40 ceramic

Figure Captions

Fig. 1. XRD patterns for TTZN carbide ceramic after spark plasma consolidation. (a) shows a refinement procedure for the TTZN–10 ceramics. (b) provide refinement of the TTZN–40 specimen. The lattice parameters for two solid solutions were: (i) a = 4.4963 Å and (ii) a = 4.4682 Å. For the volume fraction of the two phases was 42.5 and 57.5 %. (c) shows a refinement of the (442) peak. For clarity, the Kα2 peaks were not removed for (a)–(c). The bars indicate the allowed Bragg reflections for the *Fm-3m* structure. (d) shows relation between the bulk density and lattice parameters for the monolithic, binary, medium-entropy, and high-entropy carbides (using an XRD database survey) [14–16,25–29]. The difference between a general density vs lattice trend (dashed line) and that for medium-entropy/high-entropy carbides (dotted line) may indicate a more severe lattice distortion.

Fig. 2. Visual representation of medium-entropy carbide phases derived during phase refinement using a 2x2x1 supercell ($C_{16}Nb_4Ta_4Ti_4Zr_4$). An equimolar solid-solution (Nb,Zr)C via (PDF #65-8790, [28]) was visualized as a reference ($C_{16}Nb_8Zr_8$).

Fig. 3. SEM micrographs of medium-entropy carbides after flexural tests at ambient temperature: (a,b) TTZN–10, (c–e) TTZN–40. (e) shows typical microcracks observed during fracture. In order to observe homogeneity of distribution of metals with different atomic numbers in medium-entropy carbide (b,d) are provided in the BSE mode.

Fig. 4. SEM micrographs of medium-entropy carbide after flexural strength tests at elevated temperatures: (b,c) at 1000 °C, (d-g) and (h-j) 1600 °C and 1800 °C, respectively. (c, e, g, i, k) are taken in BSE mode. (a) provides a statistical variation between transgranular and intergranular fracture for all specimens tested within the present study. Dashed circles in (k) show locations of microcracks. (d, e, h, i) are TTZN–40, while (b, c, f, g, j, k) are TTZN–10.

Fig. 5. Effect of the grain size and composition of selected high-strength carbide and diboride ceramics on normalized strength values. Dashed lines provide a slope verified for tantalum diboride within study [37]. Note that the data for quaternary medium-entropy carbides in this study comport the trend for TaB_2 or TaC, but at the same time show an opposite trend, as the highest strength at room temperature has been observed for ceramics with the grain size of 19±4 μm (TTZN–10 ceramic, 566±12 MPa). This serves as a direct confirmation of the solid-solution strengthening effect. Data on binary and ternary carbides were collected in [14]. Data of ref. [16] show that decrease in grain size allows increasing strength up to by 20%.

Fig. 6. Effect of temperature on the flexural strength of TTZN carbides prepared in this study. (a) provides variation in strength for TTZN–10 ceramic, while (b) shows data for TTZN–40

ceramic and for ternary (Ta,Zr,Nb)C [14]. Dashed lines in (a) and (b) show the linear regression obtained from data in (a). (c) shows typical loading curves for TTZN–40 ceramics at 1600 °C and 1800 °C.

Fig. 7. Effect of temperature on the flexural strength of TTZN carbides and selected transition metal carbide monoliths [14, 36, 40, 41, 48–51] (see **Figures 8–12** [36,40–44,46–49,51–62] for details). Argon was used during the high-temperature flexural test for all the reported data. The closed symbols indicate that the strength was measured using a four-point setup and the open symbols show the results of the three-point flexural strength tests. Shaded area underlines sufficient increase in strength between 25 °C and 1600 °C obtained for ceramics with carbide solid-solid solutions, see **Figure 6 (b)** for clarity.

Fig. 8. Effect of temperature on the flexural strength of monolithic titanium carbide ceramics [40–44,52]. The semi-closed symbols indicate that the strength was measured using a four-point setup and the open symbols show the results of the three-point flexural strength tests. If available, average grain size (G.S.) values are presented

Fig. 9. Effect of temperature on the flexural strength of monolithic zirconium carbide ceramics [44,46,51,53,54]. The semi-closed symbols indicate that the strength was measured using a four-point setup and the open symbols show the results of the three-point flexural strength tests. If available, the average grain size (G.S.) values are presented.

Fig. 10. Effect of temperature on the flexural strength of monolithic hafnium carbide ceramics [55–57]. All reported data were collected using three-point flexural strength test. If available, the average grain size (G.S.) values are presented.

Fig. 11. Effect of temperature on the flexural strength of monolithic niobium carbide ceramics [48,49,51,52,58]. All reported data were collected using three-point flexural strength test. If available, the average grain size (G.S.) values are presented.

Fig. 12. Effect of temperature on the flexural strength of monolithic tantalum carbide ceramics [36, 59–62]. All reported data were collected using three-point flexural strength test. If available, the average grain size (G.S.) values are presented.

Fig. 13. Effect of ceramic composition on elastic moduli and specific stiffness of commonly used high-temperature ceramics. Values for stiffness at 1600 °C were estimated using approach provided in ref. [68], while the data for carbide ceramics show the Young's modulus corrected to zero porosity. HE – stands for high-entropy carbides based on data of ref. [19], while TTZ stands for $(Ta_{1/3}Zr_{1/3}Nb_{1/3})C$ [14]. Note, that the quaternary medium-entropy carbides have a minor modulus decrease at 1600 °C.

Figures

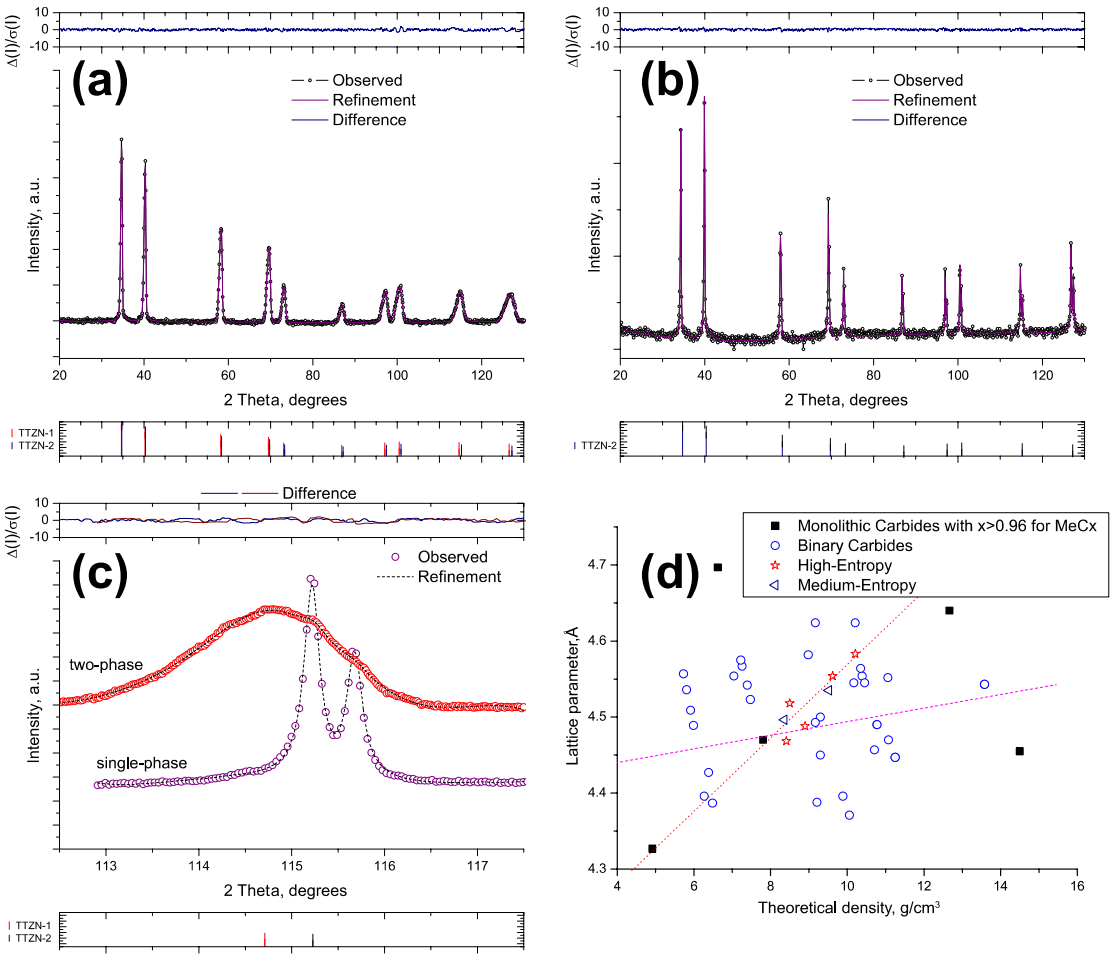

Fig. 1. XRD patterns for TTZN carbide ceramic after spark plasma consolidation. (a) shows a refinement procedure for the TTZN–10 ceramics. (b) provide refinement of the TTZN–40 specimen. The lattice parameters for two solid solutions were: (i) a = 4.4963 Å and (ii) a = 4.4682 Å. For the volume fraction of the two phases was 42.5 and 57.5 %. (c) shows a refinement of the (442) peak. For clarity, the Kα2 peaks were not removed for (a)–(c). The bars indicate the allowed Bragg reflections for the *Fm-3m* structure. (d) shows relation between the bulk density and lattice parameters for the monolithic, binary, medium-entropy, and high-entropy carbides (using an XRD database survey) [14–16,25–29]. The difference between a general density vs lattice trend (dashed line) and that for medium-entropy/high-entropy carbides (dotted line) may indicate a more severe lattice distortion.

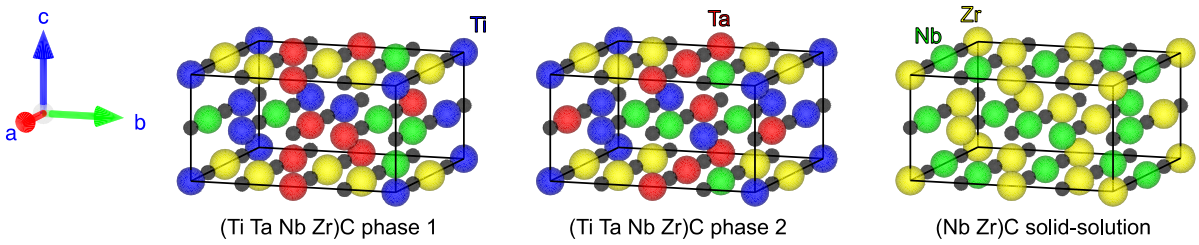

Fig. 2. Visual representation of medium-entropy carbide phases derived during phase refinement using a 2x2x1 supercell ($C_{16}Nb_4Ta_4Ti_4Zr_4$). An equimolar solid-solution (Nb,Zr)C via (PDF #65-8790, [28]) was visualized as a reference ($C_{16}Nb_8Zr_8$).

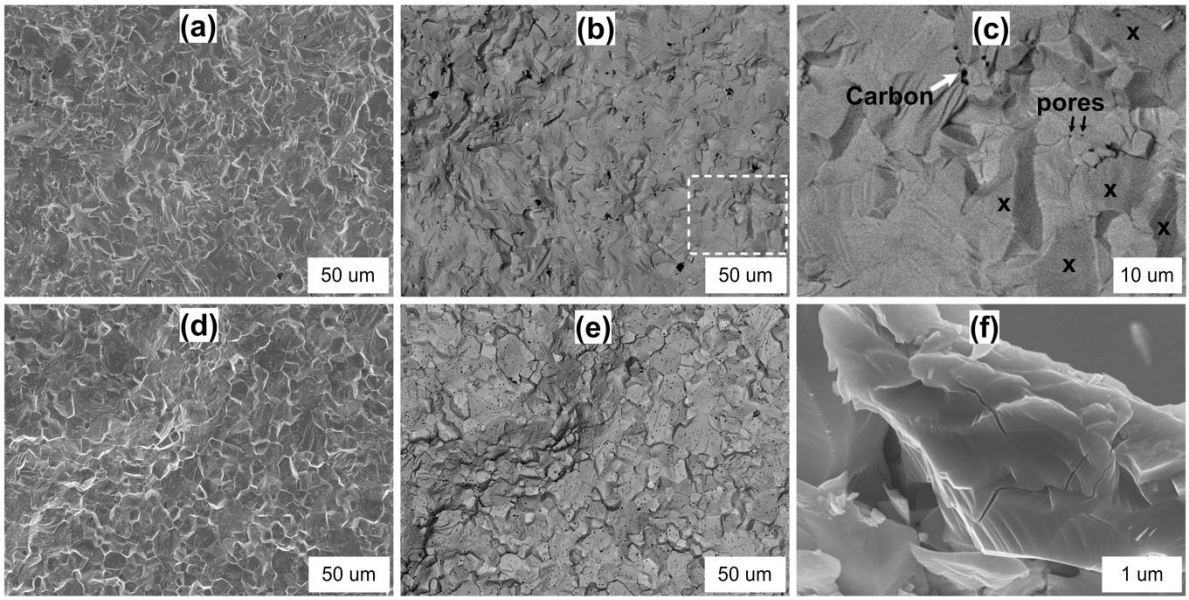

Fig. 3. SEM micrographs of medium-entropy carbides after flexural tests at ambient temperature: (a–c) TTZN–10, (d–f) TTZN–40. (f) shows typical microcracks observed during fracture. In order to observe homogeneity of distribution of metals with different atomic numbers in medium-entropy carbide (b,d,c) are provided in the BSE mode. (c) shows presence of carbon, pores and second solid-solution carbide phase (marked by x).

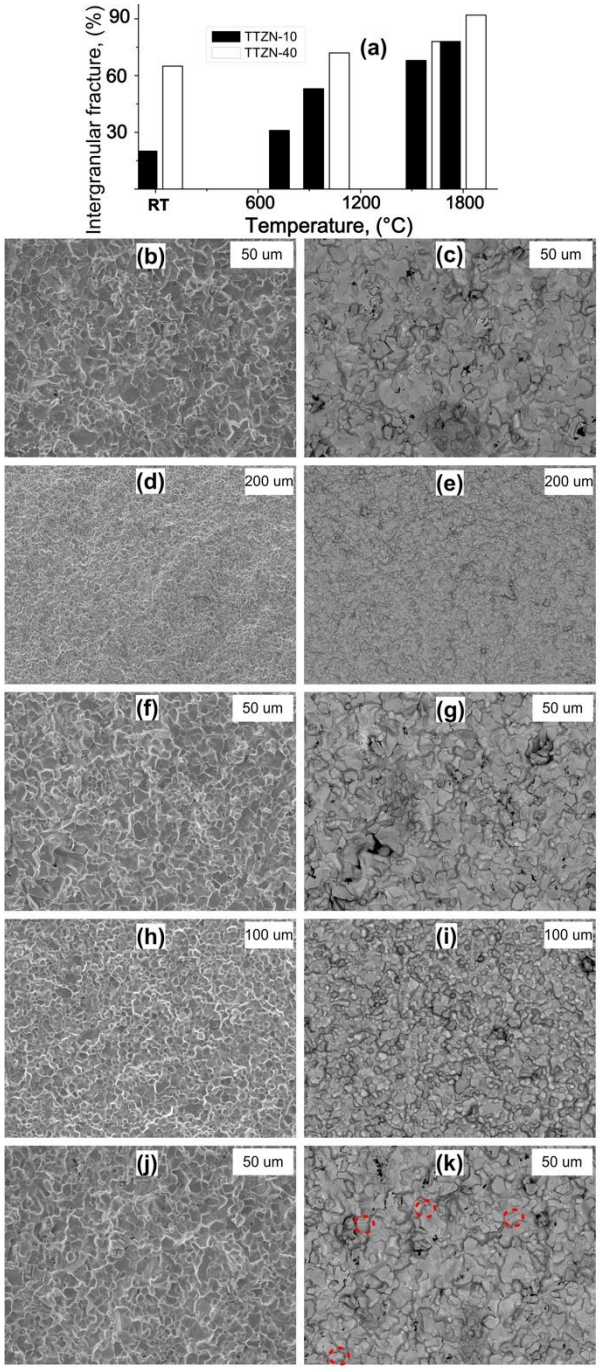

Fig. 4. SEM micrographs of medium-entropy carbide after flexural strength tests at elevated temperatures: (b,c) at 1000 °C, (d-g) and (h-j) 1600 °C and 1800 °C, respectively. (c, e, g, i, k) are taken in BSE mode. (a) provides a statistical variation between transgranular and intergranular fracture for all specimens tested within the present study. Dashed circles in (k) show locations of microcracks. (d, e, h, i) are TTZN–40, while (b, c, f, g, j, k) are TTZN–10.

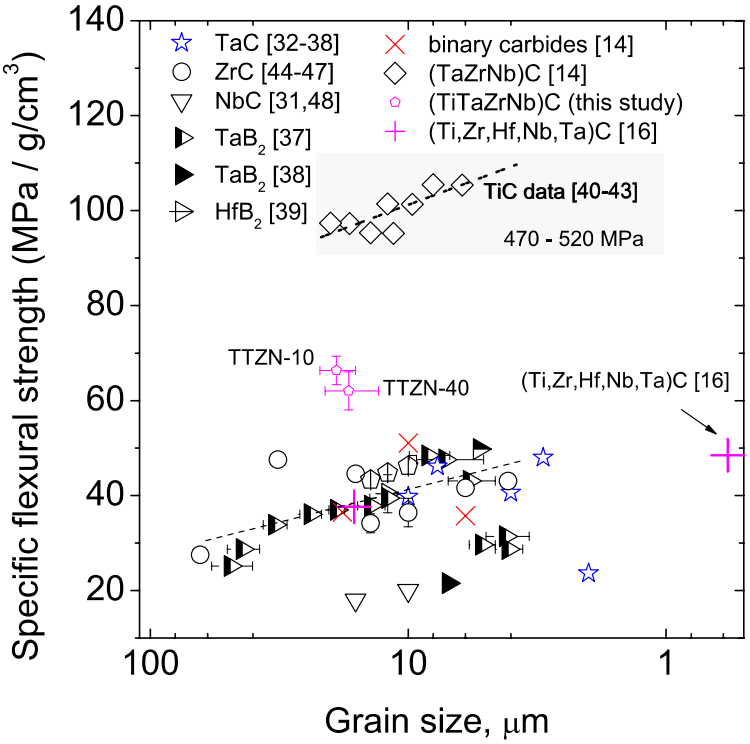

Fig. 5. Effect of the grain size and composition of selected high-strength carbide and diboride ceramics on normalized strength values. Dashed lines provide a slope verified for tantalum diboride within study [37]. Note that the data for quaternary medium-entropy carbides in this study comport the trend for TaB_2 or TaC, but at the same time show an opposite trend, as the highest strength at room temperature has been observed for ceramics with the grain size of 19±4 μm (TTZN–10 ceramic, 566±12 MPa). This serves as a direct confirmation of the solid-solution strengthening effect. Data on binary and ternary carbides were collected in [14]. Data of ref. [16] show that decrease in grain size allows increasing strength up to by 20%.

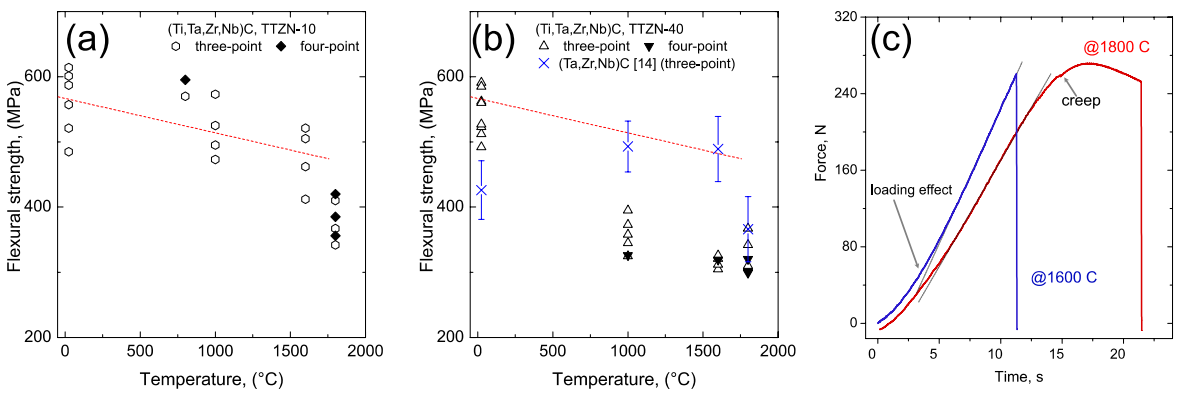

Fig. 6. Effect of temperature on the flexural strength of TTZN carbides prepared in this study. (a) provides variation in strength for TTZN–10 ceramic, while (b) shows data for TTZN–40 ceramic and for ternary (Ta,Zr,Nb)C [14]. Dashed lines in (a) and (b) show the linear regression obtained from data in (a). (c) shows typical loading curves for TTZN–40 ceramics at 1600 °C and 1800 °C.

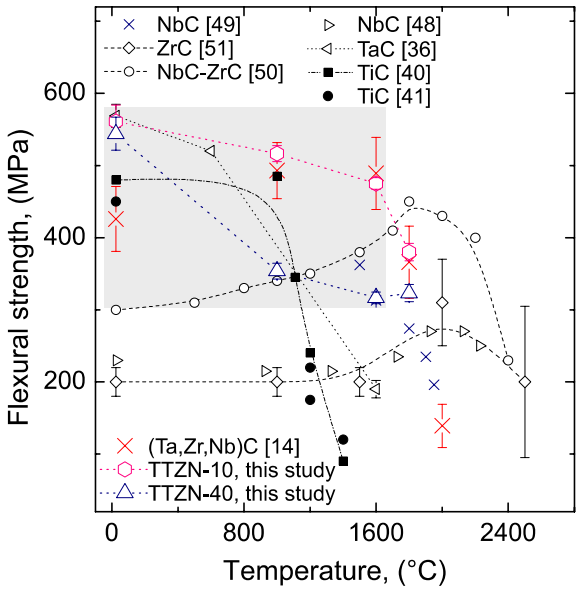

Fig. 7. Effect of temperature on the flexural strength of TTZN carbides and selected transition metal carbide monoliths [14, 36, 40, 41, 48–51] (see **Figures 8–12** [36,40–44,46–49,51–62] for details). Argon was used during the high-temperature flexural test for all the reported data. The closed symbols indicate that the strength was measured using a four-point setup and the open symbols show the results of the three-point flexural strength tests. Shaded area underlines sufficient increase in strength between 25 °C and 1600 °C obtained for ceramics with carbide solid-solid solutions, see **Figure 6 (b)** for clarity.

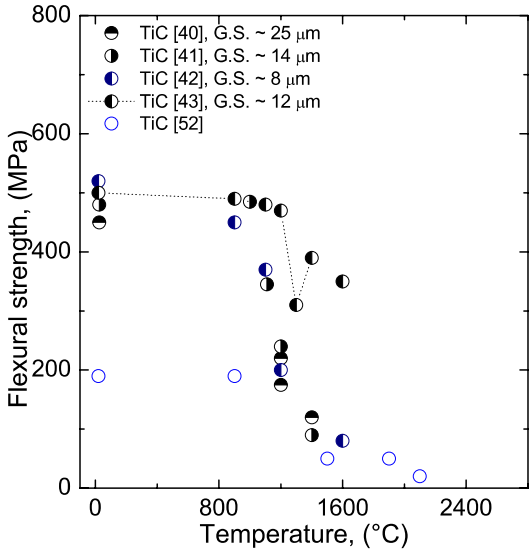

Fig. 8. Effect of temperature on the flexural strength of monolithic titanium carbide ceramics [40–44,52]. The semi-closed symbols indicate that the strength was measured using a four-point setup and the open symbols show the results of the three-point flexural strength tests. If available, average grain size (G.S.) values are presented

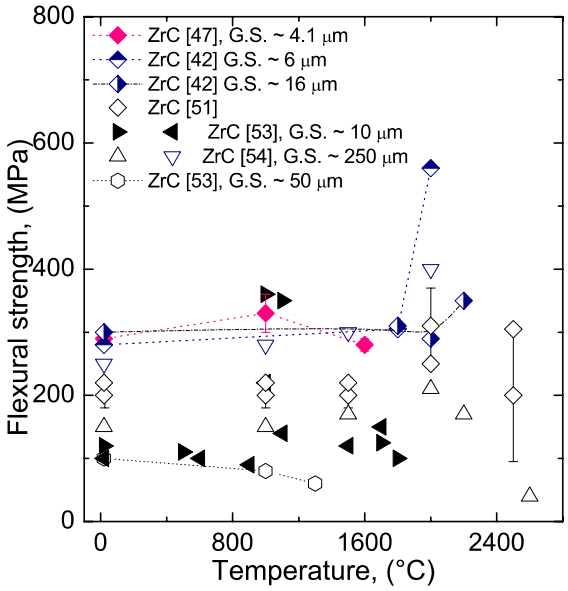

Fig. 9. Effect of temperature on the flexural strength of monolithic zirconium carbide ceramics [44,46,51,53,54]. The semi-closed symbols indicate that the strength was measured using a four-point setup and the open symbols show the results of the three-point flexural strength tests. If available, the average grain size (G.S.) values are presented.

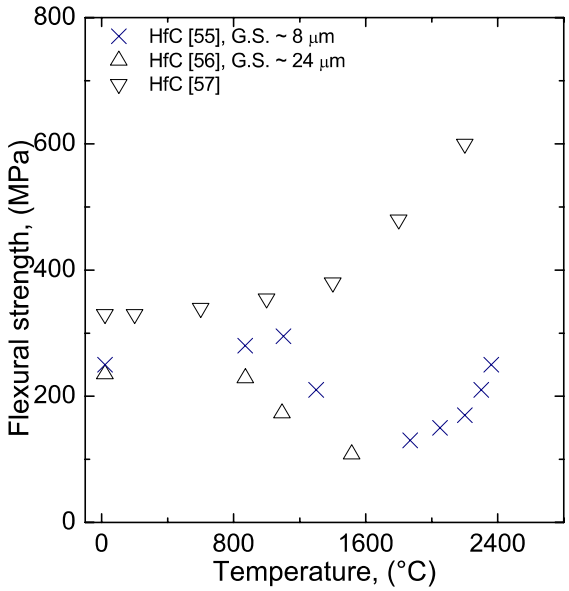

Fig. 10. Effect of temperature on the flexural strength of monolithic hafnium carbide ceramics [55–57]. All reported data were collected using three-point flexural strength test. If available, the average grain size (G.S.) values are presented.

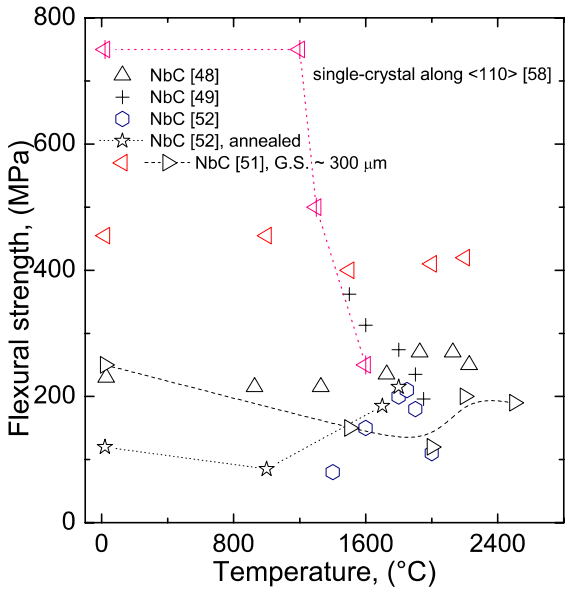

Fig. 11. Effect of temperature on the flexural strength of monolithic niobium carbide ceramics [48,49,51,52,58]. All reported data were collected using three-point flexural strength test. If available, the average grain size (G.S.) values are presented.

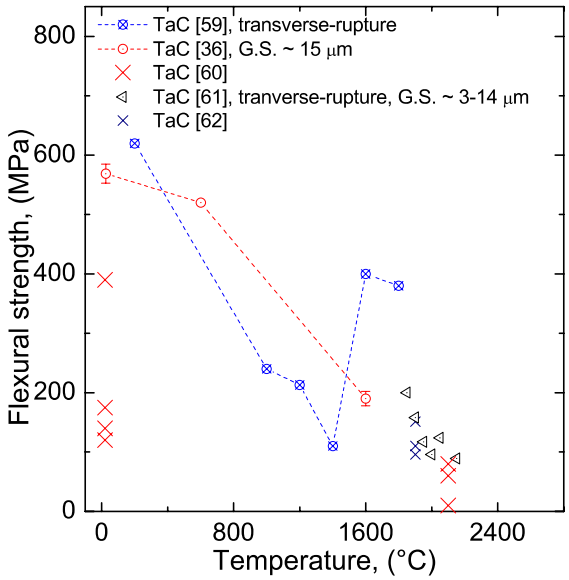

Fig. 12. Effect of temperature on the flexural strength of monolithic tantalum carbide ceramics [36, 59–62]. All reported data were collected using three-point flexural strength test. If available, the average grain size (G.S.) values are presented.

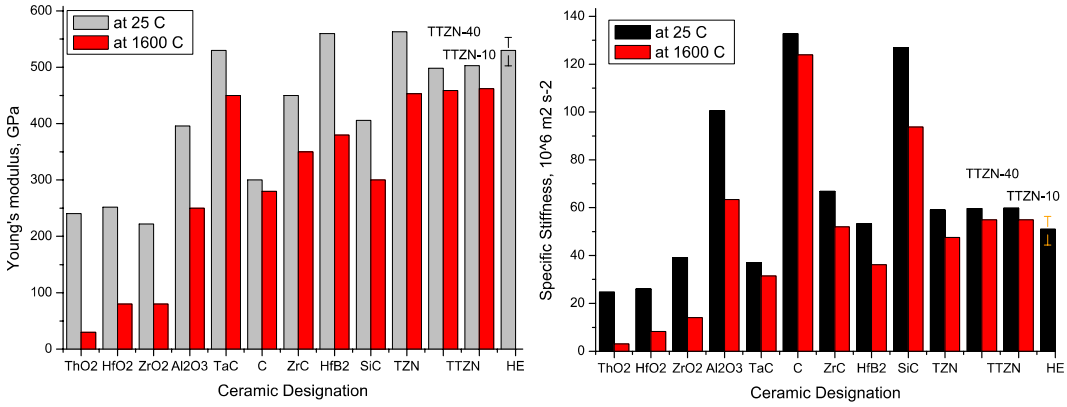

Fig. 13. Effect of ceramic composition on elastic moduli and specific stiffness of commonly used high-temperature ceramics. Values for stiffness at 1600 °C were estimated using approach provided in ref. [68], while the data for carbide ceramics show the Young's modulus corrected to zero porosity. HE – stands for high-entropy carbides based on data of ref. [19], while TTZ stands for $(Ta_{1/3}Zr_{1/3}Nb_{1/3})C$ [14]. Note, that the quaternary medium-entropy carbides have a minor modulus decrease at 1600 °C.

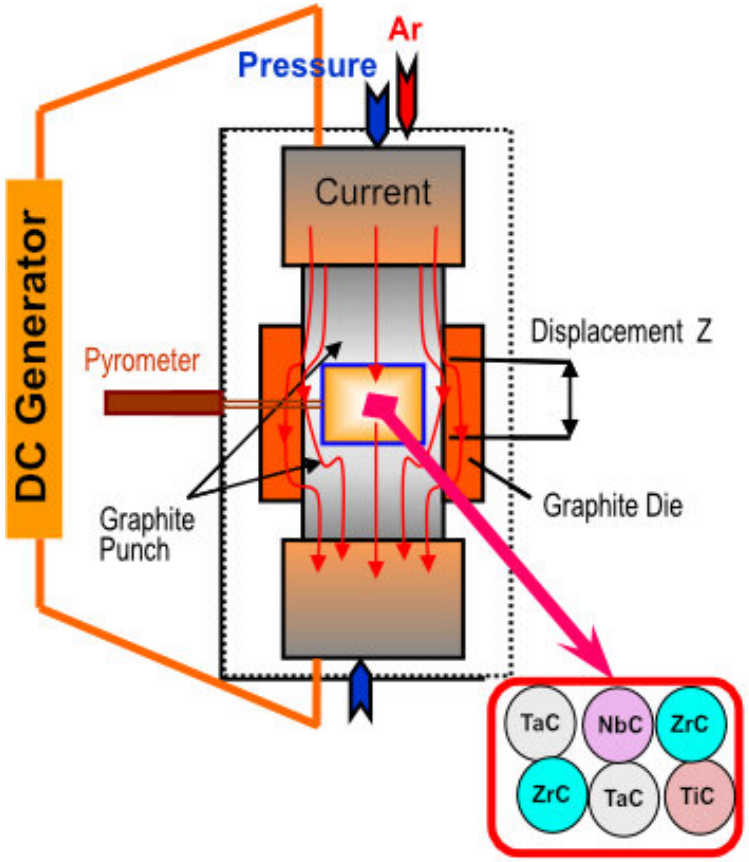

Spark plasma sintering at 1927°C

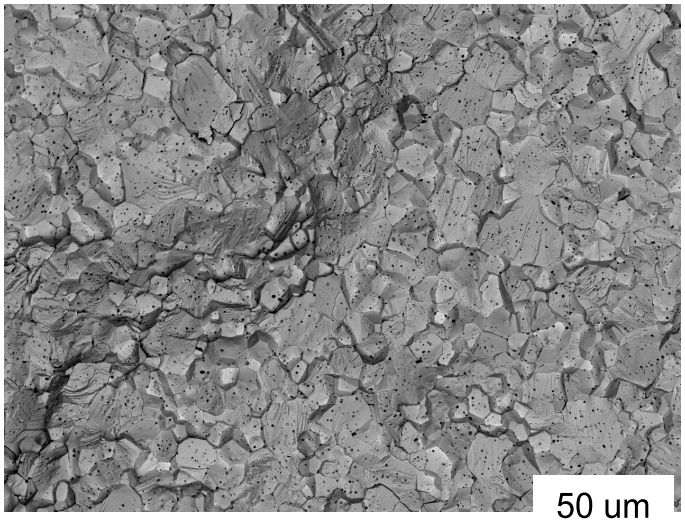

strength 320 MPa @ 1600°C

Spark plasma sintering at 1977°C

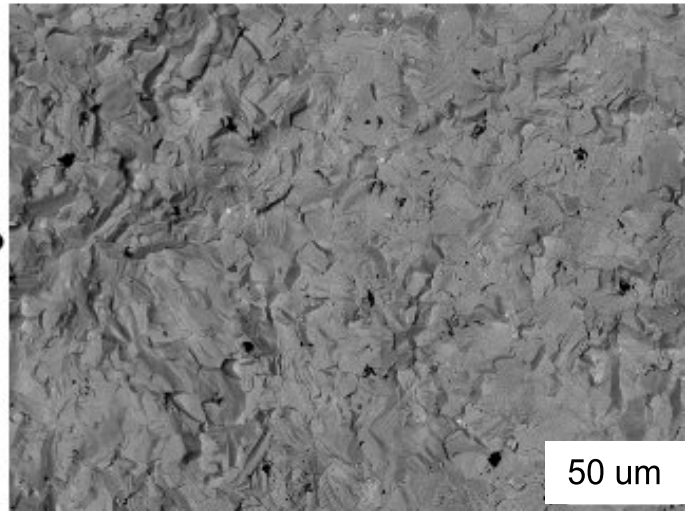

strength 475 MPa @ 1600°C